Original Article

Role of ^{18}F-FDG PET/CT in the diagnosis and management of patients with Langerhans cell histiocytosis

Zhe-Huang Luo[1#], Pu-Xuan Lu[2#], Wan-Lin Qi[1], Feng-Xiang Liao[1], Ai-Fang Jin[1], Qing-Yun Zen[1]

[1]PET/CT Center, Jiangxi Provincial People's Hospital, Nanchang, China; [2]Shenzhen Center for Chronic Disease Control, Shenzhen, China

Contributions: (I) Conception and design: ZH Luo; (II) Administrative support: ZH Luo; (III) Provision of study materials or patients: ZH Luo, WL Qi; (IV) Collection and assembly of data: ZH Luo, WL Qi, FX Liao; (V) Data analysis and interpretation: ZH Luo, PX Lu, WL Qi; (VI) Manuscript writing: All authors; (VII) Final approval of manuscript: All authors.

[#]These authors contributed equally to this work.

Correspondence to: Zhe-Huang Luo. PET/CT Center, Jiangxi Provincial People's Hospital, Aiguo Rd 152#, Donghu District, Nanchang, China. Email: lzh6392@sina.com.

Background: Langerhans cell histiocytosis (LCH) is an inflammatory myeloid neoplasm that can involve multisystem organs. Positron emission tomography/computed tomography (PET/CT) has been widely used in tumor staging and efficacy evaluation. However, at present, there are few ^{18}F-fluorodeoxyglucose (FDG) PET/CT studies on LCH. This study aimed to explore the possible role of ^{18}F-FDG PET/CT in the diagnosis and management of patients with LCH.

Methods: ^{18}F-FDG PET/CT images of 22 Chinese patients diagnosed with LCH on biopsy or surgery histopathology between January 2011 and December 2020 were retrospectively analyzed. The incidence of LCH in each system was assessed by a PET/CT scan. The imaging characteristics were analyzed semiquantitatively and qualitatively. The discrepancies between PET/CT and conventional imaging modalities were recorded. Evaluations of curative effect according to RECIST1.1 and PERCIST1.0 were compared using Fisher's exact chi-squared test, and P values <0.05 were considered significant.

Results: Eight (36.4%) of the 22 patients presented with single system involvement (4 isolated site involvement, 4 multiple site involvement), and 14 (63.6%) presented with multiple system involvement. Twenty-one (95.5%) patients had hypermetabolic lesions. Musculoskeletal, lymphatic, respiratory, liver, skin-soft tissue and thyroid involvement were seen in 14 (63.6%), 13 (59.1%), 5 (22.7%), 4 (18.2%), 5 (22.7%) and 1 (4.5%) patient, respectively. Cranial and facial bones were the most common sites of musculoskeletal involvement. Ten patients underwent PET/CT follow-up, and there was no significant difference in curative effect evaluations according to RECIST1.1 and PERCIST1.0. However, among the complete remission cases assessed by RECIST1.1, three were partial metabolic responses assessed by PERCIST1.0, while among the partial response cases assessed by RECIST1.1, one was metabolic progressive disease assessed by PERCIST1.0.

Conclusions: ^{18}F-FDG PET/CT is an imaging modality option for the diagnosis and assessment of the curative effect of LCH.

Keywords: Langerhans cell histiocytosis (LCH); ^{18}F-fluorodeoxyglucose (FDG); positron emission tomography/computed tomography (PET/CT); imaging manifestation; evaluation of therapy efficiency

Submitted Aug 19, 2021. Accepted for publication Jan 04, 2022.
doi: 10.21037/qims-21-823
View this article at: https://dx.doi.org/10.21037/qims-21-823

Introduction

Langerhans cell histiocytosis (LCH) is an inflammatory myeloid neoplasm characterized by clonal proliferation of Langerhans cells in various organs, including skin, bones, lymph nodes, soft tissue, lung and liver. LCH can occur in all age groups, but the first onset of this disorder tends to occur in children (1,2). Conventional imaging modalities such as X-ray, computed tomography (CT) and magnetic resonance imaging (MRI) play a key role in LCH not only in diagnosis and evaluating the extent of involvement but also in guiding biopsy and follow-up (2-5), and ^{18}F-fluorodeoxyglucose (^{18}F-FDG) positron emission tomography/computed tomography (PET/CT) has also been increasingly used (4,6,7). ^{18}F-FDG PET/CT has two advantages in the diagnosis and management of LCH: first, it is a whole-body study in a one-time scan; second, it provides not only anatomical details but also metabolic informations of lesions. However, because of the rarity of LCH, few studies have focused on PET/CT manifestations and assessed the curative effect of LCH, and most articles are case reports. Therefore, recognizing PET/CT findings and metabolic characteristics in different organs with LCH is a crucial element in the workflow of diagnosis and treatment of LCH. In this study, we reviewed the ^{18}F-FDG PET/CT data of 22 patients with LCH diagnosed by biopsy and/or histopathology. The PET/CT imaging findings of each organ with LCH were systemically analyzed, and evaluations of curative effect by RECIST1.1 and PERCIST1.0 were compared in 10 patients with follow-up PET/CT imaging after treatment. This study aimed to explore PET/CT image features and the role of ^{18}F-FDG PET/CT in the diagnosis and management of patients with LCH. We present the following article in accordance with the STROBE reporting checklist (available at https://qims.amegroups.com/article/view/10.21037/qims-21-823/rc).

Methods

The study was conducted in accordance with the Declaration of Helsinki (as revised in 2013) and approved by the Institutional Ethics Committee of Jiangxi Provincial People's Hospital. Individual consent for this retrospective analysis was waived.

Patient population

^{18}F-FDG PET/CT imaging findings of 22 Chinese patients diagnosed pathologically with LCH from January 2011 to December 2020 at our hospital were retrospectively analyzed. Patients who did not undergo PET/CT scans before treatment were not enrolled in this study (*Figure 1*). Follow-up for all patients was a minimum period of 1 year after the baseline PET/CT scan. The follow-up methods included telephone follow-up, WeChat follow-up and outpatient examination. The demographic information, clinical presentations, time between the first visit and PET/CT imaging, sites of biopsy and/or surgical spots and PET/CT findings of the patients were recorded. The discrepancies between PET/CT findings and conventional imaging findings were described.

Histopathology was used to verify LCH for the ^{18}F-FDG PET/CT findings. The diagnosis of LCH was made according to histopathological and immunohistochemical findings combined with the appropriate clinical and imaging context. At least one lesion was pathologically and immunohistochemically confirmed as LCH. Focal metabolic changes in follow-up PET/CT scans were also suggestive of LCH lesions.

PET/CT imaging and interpretation

All patients in this study underwent ^{18}F-FDG PET/CT before treatment. Patients fasted for at least 4 h before ^{18}F-FDG injection. Each patient, whose blood sugar level was less than 10 mmol/L, was injected intravenously with an activity of 5.5–7.4 MBq/kg ^{18}F-FDG. Patients rested for a scheduled 45–60-minute uptake period followed by image acquisition on PET/CT systems (GE Healthcare Discovery STE, USA). Patients urinated before the acquisition of images, and no oral or intravenous contrast was administered. PET/CT scans were acquired from the vertex of skull to the upper thigh with the patient supine.

PET/CT images were reviewed on a picture-archiving and communication system (PACS) workstation (GE AW 4.6 workstation) displaying a maximum-intensity projection image (MIP) and multiplanar PET, CT, and PET/CT fusion images and analyzed visually and semiquantitatively with the measurement of the maximum standardized uptake value (SUVmax). ^{18}F-FDG PET/CT findings were interpreted by 2 board-certified radiologists with more than 10 years of experience in whole-body PET/CT analysis. All focal uptakes greater than background that were not explained by physiological mechanisms were considered to be indicative of LCH lesions. In patients with multisystem involvement or multiple lymph node involvement, high diffuse uptake of

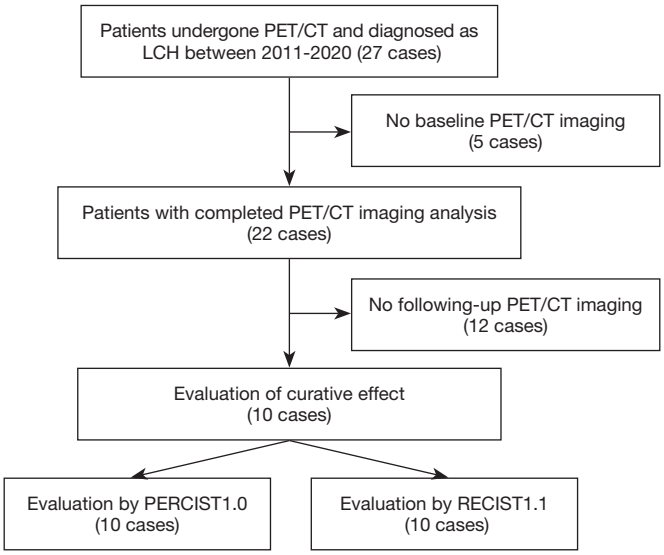

Figure 1 Flowchart of the study. PET/CT, positron emission tomography/computed tomography; LCH, Langerhans cell histiocytosis; PERCIST, PET Response Criteria in Solid Tumors; RECIST, Response Evaluation Criteria in Solid Tumors.

FDG in the spleen was considered spleen LCH involvement.

PET/CT imaging features were explored, including the number of affected organs or systems, number of lesions in each organ or tissue, SUVmax of each lesion, and morphologic CT characteristics such as shape, size, and density. The SUV of the lesions was measured by one-click measurement of workstation AW4.6.

All conventional imaging data of the patients were obtained not more than 2 weeks before the PET/CT scan, and the discrepancies between PET/CT findings and conventional imaging findings were also recorded.

Evaluation of curative effect

Curative effect were evaluated according to RECIST 1.1 (recorded as complete remission, partial remission, stable disease and progressive disease) and PERCIST 1.0 [recorded as complete metabolic remission, partial metabolic remission, stable metabolic disease and progressive metabolic disease (PMD)] in all patients who underwent PET/CT imaging before and after treatment simultaneously, and the results were compared with each other. To reduce the efficacy assessment bias for both criteria, patients' other imaging examinations (CT and/or MRI, radiography and scintigraphy) for RECIST1.1 assessment were completed within 3 days before or after PET/CT follow-up. Diagnostic CTs performed at the same time as the PET/CT examination were also referenced when evaluating curative effect by RECIST1.1.

Statistical analysis

Statistical analysis was performed using SPSS 17.0 software (SPSS/IBM, Chicago, IL, USA). The measurement data were reported as the mean ± standard deviation. The minimum, maximum, mean and proportion were used to present categorical data. Evaluations of curative effect according to RECIST1.1 and PERCIST1.0 were compared using Fisher's exact chi-squared test, and P values <0.05 were considered significant.

Results

Study population

From January 2011 to December 2020, a total of 27 patients with proven LCH underwent PET/CT imaging in our hospital, 13 patients with biopsy-diagnosed LCH and 9 patients with surgery-diagnosed LCH were enrolled (13 female, 9 male, 10 patients underwent PET/CT follow-up), and 5 patients who did not undergo PET/CT imaging prior to treatment were excluded (*Figure 1*). Of the 22 patients, 14 patients were <18 years old, and 8 were ≥18 years old (median age, 10 years; age range, 1–66 years); the time interval between the first visit and the first PET/CT

Table 1 Clinical data and biopsy/surgery sites of 22 patients with LCH

No.	Sex	Age (years)	Manifestations	Time interval (m)	Conventional imaging (before PET/CT)	Involvement site on PET/CT images	Biopsy/surgery sites
1	M	13	Right upper quadrant pain	1	Ab-CT, Ultra	Liver, abdominal LNs	Liver
2	F	6	Skin rashes	1	Ultrasound	Skin, cervical LNs	Skin, LN
3	M	2	Sternal nodule, bone pain	1	Ch-CT	Bones, cervical LNs, thymus, spleen	Sternum (S), LN
4	F	35	Bone pain	3	H-CT, Ch-CT, B-scan, Ultra	Bones, systemic LNs, spleen	Cervical LN
5	F	1	Facial bump	2	X, Head-CT	Bone, lung, cervical LNs	Facial lump
6	F	47	Neck bump	5	H-CT, Ch-CT, Ultra	Cervical LNs, thyroid, liver, labium, external auditory canal	LN, perineum
7	F	1	Skin rashes, fever, otitis media	1	X, H-CT	Skin, bones, cervical LNs, thymus, lung, spleen	Skin
8	M	29	Lower back pain	11	X, Ba-CT, B-scan, MRI	Bones, cervical LNs,	Vertebra
9	F	1	Neck nodules, fever	1	Ab-CT, Ultra	Systemic LNs, spleen	LN
10	F	1	Exophthalmus	3	H-CT	Orbital wall soft tissue, cervical LNs	Soft tissue (S)
11	F	58	Head nodule	6	H-CT	Bone	Skull (S)
12	M	2	Head nodule	3	H-CT, Ch-CT	Bones	Skull (S)
13	M	66	Cough, distress, shortness of breath	5	X, Ch-CT	Lung	Lung
14	F	60	Head nodule	6	X, H-CT	Bone	Skull (S)
15	F	33	Chest pain, chest nodule	2	Ch-CT	Bone	Rib (S)
16	F	1	Head nodule	1	H-CT, Ch-CT	Bones, systemic LNs, liver	Skull
17	M	17	Bone pain	2	X, Ch-CT MRI	Bone, lung	Vertebra (S)
18	M	15	Destress and shortness of breath, chest pain	6	X, Ch-CT	Lung	Lung
19	M	51	Bone pain	2	X, H-CT	Bone, mediastinal LNs	Clavicle
20	F	7	Skin rashes	4	X	Skin, bone	Skin (S)
21	F	7	Bone pain	1	X, CT	Bone	Scapula (S)
22	M	3	Abdominal pain	1	Ab-CT, Ultra	Liver, abdominal LNs	Liver

LCH, Langerhans cell histiocytosis; Y, years old; m, months; M/F, male/female; time interval, period between the first visit and first PET/CT imaging; LN, lymph node; Ab, abdominal; Ultra, ultrasound; Ch, chest; H, head; B, bone; X, X-ray survey; Ba, basin/pelvis; S, surgery; PET/CT, positron emission tomography/computed tomography.

imaging ranged from 1 to 11 months. The most common complaints were pain, peripheral lymphadenopathy, nodules or bumps. The most common biopsy/surgery sites were bone. Among the 22 patients, 8 (36.4%) presented with single-system/organ LCH, which involved a single site in 4 cases and multiple sites or organs in 4 cases, and 14 (63.6%) had multisystem involvement (*Table 1* and *Figure 2*).

^{18}F-FDG PET/CT findings

The most common sites of involvement were the skeletal system (63.6%, 14/22) and lymph nodes (LN, 59.1%, 13/22). ^{18}F-FDG PET/CT was positive in 21 patients (95.5%), revealing the presence of at least one hypermetabolic lesion consistent with LCH. Only in one patient with pulmonary LCH, no lesion with FDG uptake was observed.

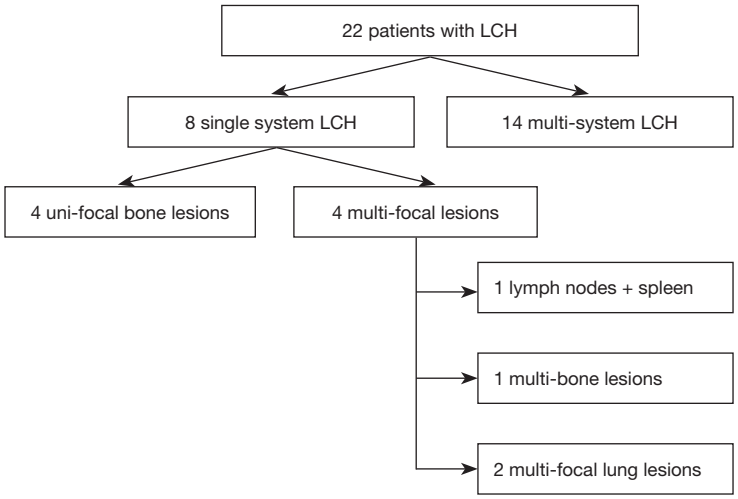

Figure 2 LCH classification of 22 patients. LCH, Langerhans cell histiocytosis.

Table 2 Sites of bone LCH involvement

No.	Sites of bone involvement					
	Cranial (C), facial (F)	Spinal column	Clavicle (Cl), scapula (Sc), sternum (St), ribs (R)	Hip bone	Humerus (H), ulna (U)	Femur (Fe), tibia (Ti)
3	C	L3	St			
4	C	T8	St	Ilium		
5	C, F					
7	C, F					
8		L5, S		Ilium		Fe
11	C					
12	C		R	Ilium	H, U	Fe
14	C					
15			R			
16	C	C5, T8, T12, L2, L4	R	Ilium		Fe
17		C6				
19	C		Cl			
20						Ti
21			Sc			

LCH, Langerhans cell histiocytosis. In the spinal column: L, lumbar, T, thoracic, S, sacral, and C, cervical.

Bone involvement

Fourteen of the 22 (63.6%) patients with LCH had bone involvement. The numbers of patients with lesions in cranial and facial bones; the spine; scapula, clavicle, sternum and ribs; hip bones; the humerus and ulna; and the femur and tibia were 9 (40.9%); 5 (22.7%); 7 (31.8%); 4 (18.2%); 1 (4.5%); and 4 (18.2%), respectively (*Table 2*, *Figure 3*). Cranial and facial bones were the most commonly involved sites.

Osteolytic lesions were observed in 14 (63.6%) patients;

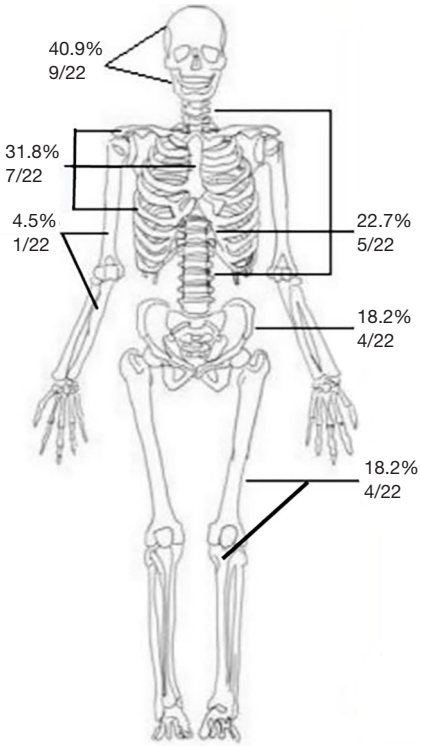

Figure 3 Distribution of bone lesions in 22 patients with Langerhans cell histiocytosis. The most commonly affected regions were cranial and facial bones.

meanwhile, osteosclerotic lesions were observed in 4 (18.2%) patients, including 3 mixed lytic-sclerotic (lytic center and sclerotic rim) lesions. All lesions were well circumscribed, and the typical radiographic findings were osteolytic lesions with associated soft tissue-like nodules/masses (*Figure 4*, Figure S1). All lesions of the skull involved the inner and outer plates. No corresponding intervertebral disc involvement was observed in 5 patients with vertebral involvement.

A total of 49 bone lesions (BLs) with LCH localizations were detected; 42 lesions were osteolytic, 5 were osteosclerotic, and 2 had confirmed hypermetabolic LCH BLs and no corresponding changes in other imaging modalities (X-ray survey, CT scans). Among the 49 BLs, 19 (38.8%) were found in the craniofacial bones, 10 (20.4%) in the column, 2 (4.1%) in sternum, 3 (6.1%) in the ribs, 6 (12.2%) in the ilium, 1 (2.0%) in the scapula, 1 (2.0%) in the clavicle, 1 (2.0%) in the humerus, 1 (2.0%) in the ulna, 4 (8.1%) in the femur, and 1 (2.0%) in the tibia (*Table 2*). Forty (81.6%) lesions were FDG-avid with a maximum standard uptake value (SUVmax) of 2.3–23.2 (mean, 7.2±6.1), and 9 (18.4%) lesions were not FDG-avid. BLs with associated soft tissue masses were all hypermetabolic.

Lymphatic system involvement

Thirteen (59.1%) of the 22 patients had lymphatic system involvement (*Figure 5*, Figure S2), including 3 with systemic lymph node (LN) involvement, 10 with regional LN involvement, 2 with thymus involvement and 4 with spleen involvement. LNs affected by LCH were seen most commonly in the cervical region (7 cases, 31.8%). Most of the affected LNs were enlarged and well demarcated, and some LNs fused together as a mass. All affected LNs showed high FDG uptake with a mean SUVmax of 7.6±4.7 (range, 2.3–16.4).

Four spleens showed diffuse and homogeneous FDG uptake, and the SUVmax was 1.4 (liver, 1.0), 1.7 (liver, 1.1), 1.7 (liver, 1.3) and 5.9 (liver, 1.2). The involved thymus in 2 patients was enlarged; one showed diffuse and homogeneous FDG uptake (SUVmax, 9.3), and the other showed heterogeneous FDG uptake (SUVmax, 4.6).

Respiratory system involvement

In the 22 patients with LCH, infiltration of the pulmonary parenchyma (*Figure 6*) was seen in 5 cases (22.7%). One appeared as soft tissue lesions with heterogeneous intense FDG uptake (SUVmax, 10.2) scattered bilaterally in the lungs; one showed diffuse ground-glass opacity and interlobular septal thickening with mild FDG avidity (SUVmax, 1.7) combined with cystic lesions; one revealed segmental lung collapse with mild FDG activity (SUVmax, 2.1); one displayed multiple nodules with moderate uptake (SUVmax, 4.3) combined with bilateral cystic lesions and left pneumothorax; and one had diffuse bilateral miliary nodules without significant uptake. Four patients showed pleural thickening without effusion.

Liver involvement

There were four patients (18.2, 4/22) with liver LCH involvement (*Figure 7*) in the study: one had diffuse hypodense nodules and two little cystic cavities with FDG-avidity (SUVmax, 4.6), two had several hypodense lesions without increased FDG uptake, and one showed hepatomegaly (SUVmax, 2.8).

Skin and soft tissue involvement

Of the 22 patients with LCH, 5 (22.7%) had positive

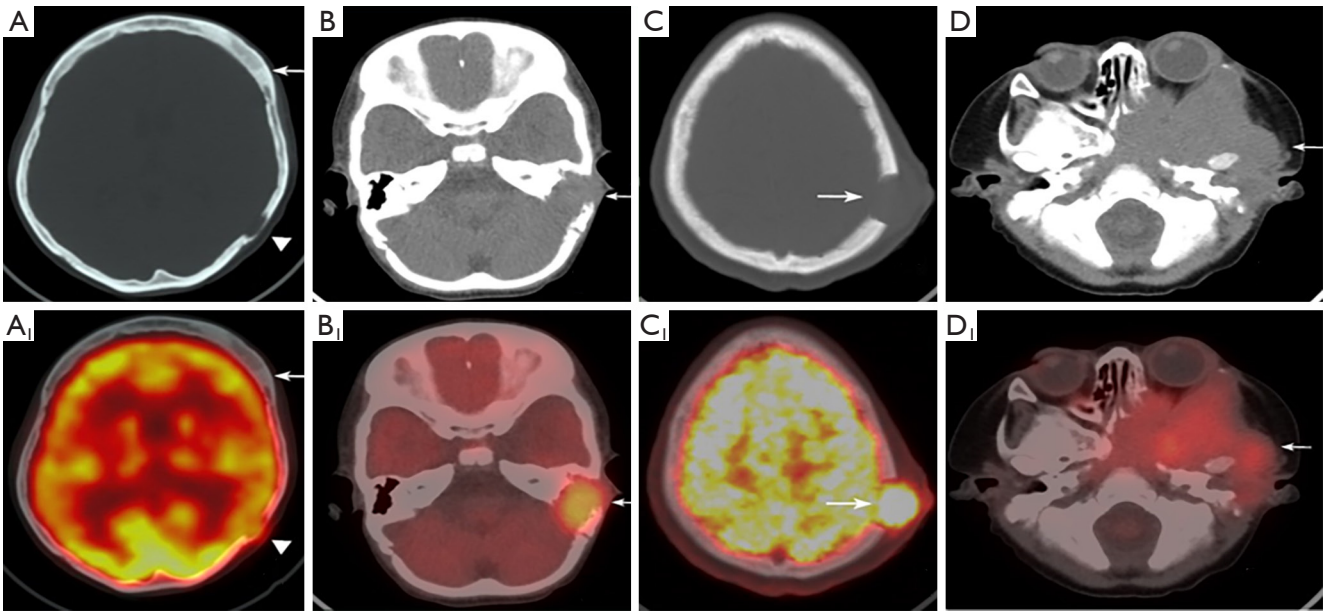

Figure 4 ^{18}F-FDG PET/CT imaging of patients with musculoskeletal involvement of LCH. (A and A_1) Axial CT (bone window) and fused image of a 35-year-old woman with LCH showing a left parietal lytic lesion with mild avidity (white triangle) and a left frontal osteogenic lesion (arrows) without FDG uptake. (B and B_1) Axial CT and fused image of a 1-year-old girl with LCH showing a left petrous lytic lesion and associated soft tissue nodule (arrows) with intense FDG uptake. (C and C_1) Axial CT (bone window) and fused image of a 58-year-old woman with LCH showing a left parietal lytic lesion and soft tissue nodule (arrows) with intense uptake. (D and D_1) Axial CT and fused image of a 1-year-old girl showing a left basal lytic lesion and mass (arrows) with media avidity of the skull base. FDG, fluorodeoxyglucose; PET/CT, positron emission tomography/computed tomography; LCH, Langerhans cell histiocytosis.

findings in soft tissue, including one with labium swelling with intensive FDG uptake (SUVmax, 5.6) and soft tissue swelling of the bilateral external auditory canal with hypermetabolism (SUVmax, 5.6) and one with orbital wall soft tissue swelling with mild FDG uptake (SUVmax, 2.6). Three patients had skin involvement without abnormal PET/CT findings.

Thyroid involvement

One patient had thyroid involvement, and the thyroid displayed enlarged and diffuse homogeneous FDG avidity (SUVmax, 10.6).

Imaging discrepancies: PET/CT vs. conventional imaging modalities

PET/CT found at least 14 more lesions than conventional imaging modalities. LCH was diagnosed by PET/CT in more organs compared with conventional imaging. The imaging discrepancies are shown in *Table 3*.

Follow-up ^{18}F-FDG PET/CT during/after treatment and evaluation of efficient response

Ten patients underwent at least one (range, 1 to 4) ^{18}F-FDG PET/CT scan during or after treatment: 3 patients with multiple-site disorder after surgery and chemotherapy, 2 with isolated BL after surgery (one cranial lesion and one rib lesion); and 5 with multisystem disease after chemotherapy. The follow-up periods ranged from 3 to 12 months. Complete and partial remission (CR, PR) accounted for 80% according to RECIST1.1, complete and partial metabolic remission (CMR, PMR) accounted for 70% according to PERCIST1.0, and there were no significant differences between the two evaluations (χ^2=0.263, P>0.05, 95% confidence interval: 0.22–13.41). However, 3 cases assessed as CR by RECIST1.1 were assessed as PMR by PERCIST1.0, and one case assessed as PR by RECIST1.1 was assessed as PMD by PERCIST1.0 (*Table 4*, Figures S2,S3).

The remaining 14 patients did not undergo PET/CT follow-up.

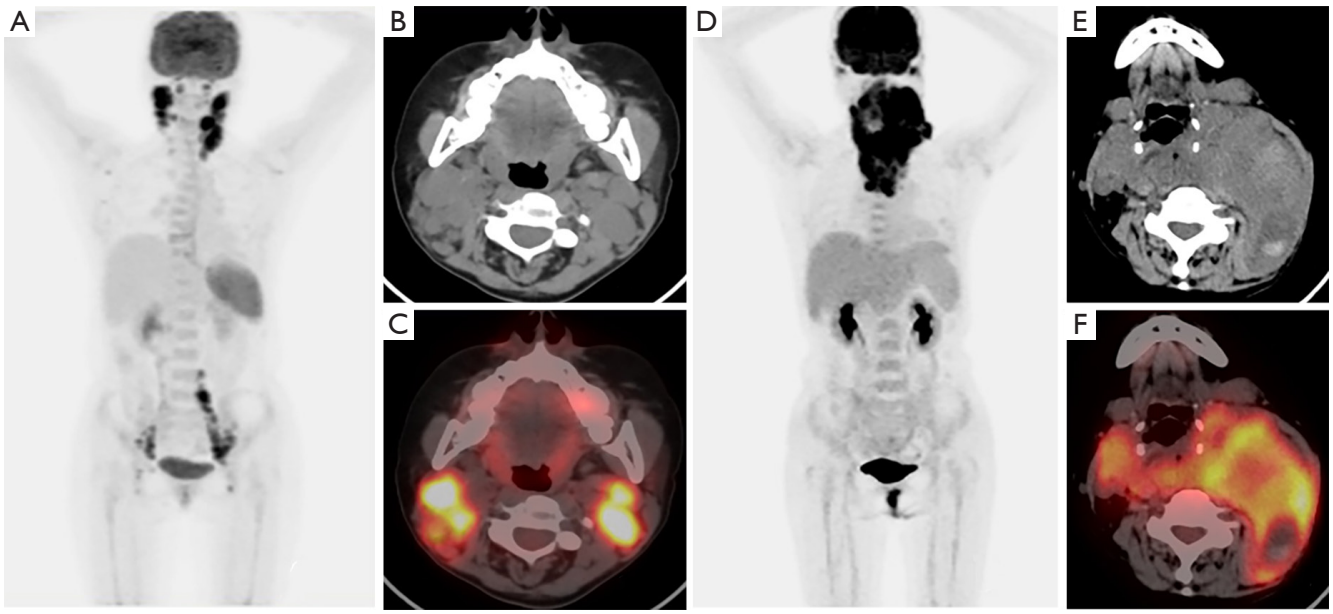

Figure 5 ^{18}F-FDG PET/CT imaging of patients with lymphatic system involvement of LCH. (A-C) Images of a 35-year-old woman (the same woman as *Figure 4A*,*4A1*) with LCH. PET MIP (A) showing multiple hypermetabolic foci in the neck and basin and a slightly enlarged spleen with increased FDG uptake. Axial CT (B) and fused image (C) displaying multiple cervical lymph nodes of varying size with intensive activity. (D-F) Images of a 47-year-old woman with LCH. PET MIP showing an intense cervical FDG-avid lesion, and axial CT (E) and fused imaging (F) showing enlarged, partially fused cervical lymph nodes with bleeding and increased FDG uptake. FDG, fluorodeoxyglucose; PET/CT, positron emission tomography/computed tomography; LCH, Langerhans cell histiocytosis; MIP, maximum-intensity projection.

Discussion

LCH belongs to a group of rare hematologic disorders characterized by abnormal clonal proliferation and accumulation of Langerhans cells (8). Its etiology remains unknown. According to the number of lesions, it is classified into two types (9): single-system LCH (sLCH) with multifocal or unifocal involvement and multisystem LCH (mLCH). Because the two types of LCHs have different therapeutic regimens and prognoses, particularly the involvement of risk organs such as the central nervous system, lung, liver, spleen and hematopoietic system, which may lead to a poor prognosis (10), it is important to distinguish between the two types of LCHs as early as possible. The evaluation of imaging before treatment plays an outstanding role. Although conventional imaging studies, such as X-ray, CT, MRI and bone scintigraphy, are recommended for the evaluation of patients with LCH (2-5), the diagnosis of LCH is still challenging, and several studies have explored the role of ^{18}F-FDG PET/CT in the diagnosis and management of LCH (6,7,9). In this study, we systematically reviewed the PET/CT findings of LCH in each system, with emphasis on systemic and rare imaging manifestations, including infiltration of lung, liver, thyroid and so on. We found that most active lesions of LCH were FDG-avid, PET/CT was useful for diagnosis of LCH and evaluating curative effect and had higher sensitivity than conventional imaging modalities, which is consistent with previous reports (11-14).

Bone is the common site of involvement (7,15). Bone involvement, either as a solitary lesion or a part of multisystem disorder, was seen in 72.7% of patients in this series. Pain was the most common complaint of patients with bone LCH at the time of their first visit (4). Previous studies comparing conventional imaging have demonstrated ^{18}F-FDG PET/CT to be more sensitive and specific for lesion detection (1,7). In this series, some early bone involvement spots had no clinical or radiographical manifestations; PET/CT scans gave distinct advantages in the diagnosis of these clinically and radiographically silent involvements, which showed FDG uptake (Figure S1); and PET/CT detected more bone LCH lesions than

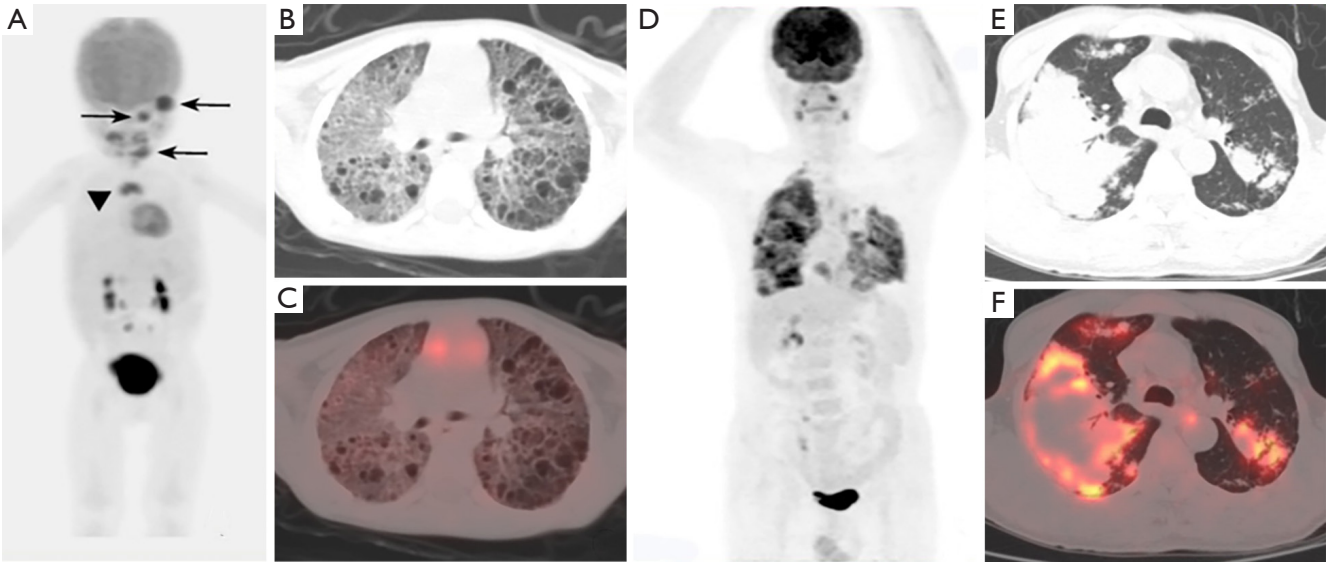

Figure 6 ^{18}F-FDG PET/CT imaging of patients with lung involvement of LCH. In a 1-year-old girl (the same girl as *Figure 4B*,*4B1*) with LCH, PET MIP (A) showing a mildly hypermetabolic chest and heterogeneous hypermetabolic thymus (black triangle); note also multiple cranial and facial FDG-avid lesions (arrows); axial CT (B) and fused image (C) revealing diffuse ground-glass opacity and cysts in bilateral lungs with mild avidity. In another 66-year-old man with LCH, PET MIP (D) showing diffuse intensive FDG uptake in the chest, and axial CT (E) and fused imaging (F) displaying multiple consolidations with heterogeneous FDG avidity in the bilateral lungs. FDG, fluorodeoxyglucose; PET/CT, positron emission tomography/computed tomography; LCH, Langerhans cell histiocytosis; MIP, maximum-intensity projection.

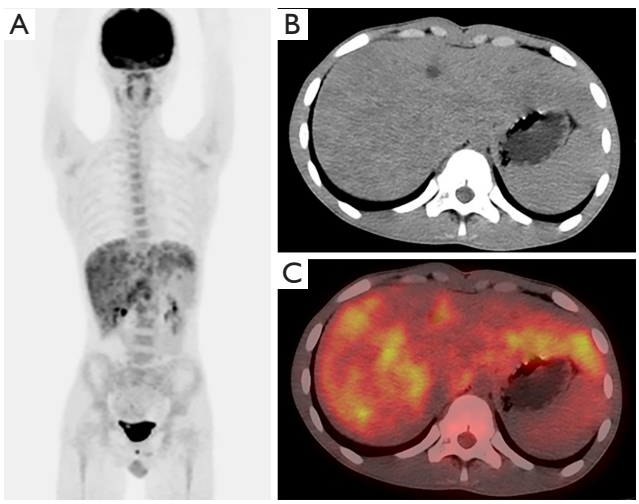

Figure 7 ^{18}F-FDG PET/CT imaging of a 13-year-old boy with liver involvement of LCH. PET MIP (A) showing diffuse heterogeneous hypermetabolic liver, axial CT (B) and fused image (C) showing diffuse hypodensity lesions (maximum diameter <3 mm) with heterogeneous FDG uptake and a 6 mm cyst. FDG, fluorodeoxyglucose; PET/CT, positron emission tomography/computed tomography; LCH, Langerhans cell histiocytosis; MIP, maximum-intensity projection.

Table 3 Imaging discrepancies: PET/CT *vs.* conventional imaging

Locations	Conventional imaging modalities		^{18}F-FDG PET/CT	
	Found lesions	Diagnosed LCH (cases)	Found lesions	Diagnosed LCH (cases)
Skeleton	47	9/14	49 (+7*)	11/14
Lymphatic system				
LNs# (areas)	24	1/13	31 (+5*)	6/13
Spleen	1	1/4	4	2/4
Thymus	1	1/2	2	1/2
Lung	4	0/5	4	1/5
Liver	4	0/4	4	0/4
Soft tissue	1	1/5	2	1/5
Thyroid	1	0/1	1	0/1

*, without final follow-up results; LNs, lymph nodes; #, 2 cervical, 2 axillary, 2 inguinal, 1 mediastinal, 1 retroperitoneal, 1 peritoneal area in the whole body. PET/CT, positron emission tomography/computed tomography; LCH, Langerhans cell histiocytosis; LN, lymph node.

Table 4 Evaluation of curative effect of 10 patients with LCH

No.	Therapeutic approach		Evaluation by RECIST1.1	Evaluation by PERCIST1.0
	Surgery	Chemotherapy		
3	+	+	PD	PMD
4		+	CR	PMR
5		+	PD	PMD
7		+	CR	PMR
9		+	PR	PMR
10	+	+	CR	CMR
12	+	+	CR	PMR
14	+		CR	CMR
15	+		CR	CMR
16		+	PR	PMD

LCH, Langerhans cell histiocytosis; RECIST, Response Evaluation Criteria in Solid Tumors; PERCIST, PET Response Criteria in Solid Tumors; PD, progressive disease; CR, complete remission; PR, partial remission; PMD, progressive metabolic disease; PMR, partial metabolic remission; CMR, complete metabolic remission.

conventional imaging. In a study published by Wu *et al.* (16), there were 81 BLs in 32 patients; CT showed 79 lesions, and PET showed 75 lesions. This suggested that the combination of PET and CT had more advantages in the discovery of bone LCH lesions.

The imaging findings of pulmonary LCH include nodular opacity, ground-glass opacity, nodules with or without lacuna, thick or thin cysts, fibrosis, etc., and the most common imaging findings were multiple nodules and cysts (3,13). Wu *et al.* (16) found that the lung was one of the most common organs involved, and all patients had characteristic chest CT scan findings. In our series, lung involvement was observed in 5 (22.7%) cases, not all patients had characteristic findings, and pulmonary LCH in one case presented with multiple consolidation and necrosis (*Figure 6E,6F*), which is exceedingly rare and has not been shown before to the authors' knowledge. This suggests varying imaging findings of pulmonary LCH. PET/CT

evaluation did not show an advantage over conventional imaging in finding pulmonary lesions; however, it can comprehensively assess the range of LCH involvement in the whole body. Furthermore, PET/CT revealed active or inactive lesions that are significant to guiding LCH biopsy, staging and therapeutic regimens (17). Some patients with LCH may have other pulmonary disorders with FDG uptake, and differential diagnostic dilemmas may arise. However, pulmonary LCH lesions were characterized by ill-defined or stellate nodules, bizarre-shaped cysts, and reticular or nodular opacities. Pleural thickening was observed in 4 out of 5 patients with pulmonary LCH, and no pleural effusion was observed, which may be a key point distinguishing it from other diseases.

The imaging findings of hepatic LCH are diverse and easily misdiagnosed, and solitary liver involvement is quite uncommon (18). One liver in this series had multiple hypodense nodules that mimicked metastasis; cysts were seen in 1 case, cystic hepatic LCH may masquerade as multiple hepatic cysts or Caroli's disease (19), but metastasis and Caroli's disease usually have no LCH lesions of other organs. Hepatic LCH is considered to progress through the following four phases: proliferative, granulomatous, xanthomatous, and fibrous phases (20). The hypercellularity of the granulomas is responsible for hypermetabolism of nodules and walls of cavities, and ^{18}F-FDG PET/CT showed the lesion phase well.

LN involvement in LCH has been previously recorded in the literature (13,21). In the 22 patients, 63.6% of the cases were multisystemic disorders. In addition to the bones, LNs were also major sites of LCH involvement, and almost all were part of systemic disease, although they can be isolated lesions of LCH. The affected LNs showed intense FDG uptake; however, this is nonspecific, and it is difficult to differentiate from other lymphadenopathies, such as lymphatic metastasis, lymphoma, and tuberculous lymphadenitis. In our study, much of the lymph node LCH involvement was missed before PET/CT, mainly due to the neglect of lymphatic system involvement and rarely targeted examination of the lymph nodes. Whole-body PET/CT examination improved the overall assessment of the lymph nodes.

Similar to lymphadenopathy, the imaging findings of thymus, spleen, and soft tissue involvement were also nonspecific. Based on this study, as a whole-body examination, combined with the finding of other organs, such as bone, lung or liver, LCH involvement, PET/CT was helpful for arriving at a possible diagnosis and improved the diagnostic accuracy of involvement in some systems and organs.

In addition, LCH patients lack specific laboratory markers for assessing curative effect. Studies (13,21) have demonstrated that PET/CT is superior to conventional imaging in assessing curative effect in patients with malignancy. In this study, PET/CT follow-ups of 10 patients with LCH suggested that metabolic changes preceded morphological changes to curative effect regardless of whether LCH was in remission or progressed. Although organ involvement is an important prognostic factor for LCH, after our observations, metabolic tumor volume seemed to be more significant for prognostic evaluation; validation studies are required in future large-sample studies. Moreover, patients with isolated bone involvement of LCH had a good postoperative prognosis in our group, and we think these patients need not be recommended for PET/CT imaging follow-up.

It is necessary to comprehensively explore whole-body lesions using various imaging modalities and clinical findings (4). Compared with traditional imaging, we believe that the survey and efficacy evaluation of multisystemic or multifocal LCH mainly rely on PET/CT examination.

Due to the rarity of LCH, the sample size of this study was small, and not all LCH patients underwent PET/CT examination before and after treatment. The advantages of PET/CT in the efficacy evaluation of LCH may not be fully reflected. Furthermore, guidelines for the use of PET/CT in LCH management have not been established. In fact, unifocal bone involvement is the least severe form of LCH and has good outcomes of treatment; more than 80% of patients completely recover (22). These patients perhaps do not require PET/CT follow-up.

A recent study suggested the involvement of the PD-1/PD-L1 immune checkpoint system in the pathogenesis of musculoskeletal LCH (23). This may provide new hope for targeted therapy for LCH. An increasing number of targeted drugs are likely to be developed. PET/CT can be used to evaluate the efficacy of new drugs and will also play a key role in the development of new drugs to treat LCH.

Conclusions

Most LCH lesions were FDG-avid. Although bone LCH lesions usually have typical imaging features, ^{18}F-FDG PET/CT shows more clinically and radiographically silent bone LCH lesions. Partial pulmonary and hepatic LCH lesions also had characteristics. However, there were many LCH lesions without typical or specific imaging manifestations in various organs and tissues. Through a

whole-body PET/CT scan, the diagnostic accuracy of systemic LCH was improved, and the extent of LCH involvement was comprehensively and systemically assessed. Moreover, PET/CT showed the metabolic activity of lesions and provided a more accurate assessment of curative effect than conventional imaging. PET/CT is an imaging modality option for the diagnosis and evaluating curative effect of LCH. Although PET/CT has been increasingly used for LCH management, not all patients need to be referred to PET/CT scans, such as in cases of solitary site involvement. Because PET/CT is expensive and involves radiation exposure, guidelines should be established for the use of ^{18}F-FDG-PET/CT scans in LCH management.

Acknowledgments

Funding: None.

Footnote

Reporting Checklist: The authors have completed the STROBE reporting checklist. Available at https://qims.amegroups.com/article/view/10.21037/qims-21-823/rc

Conflicts of Interest: All authors have completed the ICMJE uniform disclosure form (available at https://qims.amegroups.com/article/view/10.21037/qims-21-823/coif). The authors have no conflicts of interest to declare.

Ethical Statement: The authors are accountable for all aspects of the work in ensuring that questions related to the accuracy or integrity of any part of the work are appropriately investigated and resolved. The study was conducted in accordance with the Declaration of Helsinki (as revised in 2013). The study was approved by the Institutional Ethics Committee of Jiangxi Provincial People's Hospital, and individual consent for this retrospective analysis was waived.

References

1. Ferrell J, Sharp S, Kumar A, Jordan M, Picarsic J, Nelson A. Discrepancies between F-18-FDG PET/CT findings and conventional imaging in Langerhans cell histiocytosis. Pediatr Blood Cancer 2021;68:e28891.
2. Barkaoui MA, Queheille E, Aladjidi N, Plat G, Jeziorski E, Moshous D, et al. Long-term follow-up of children with risk organ-negative Langerhans cell histiocytosis after 2-chlorodeoxyadenosine treatment. Br J Haematol 2020;191:825-34.
3. Della Valle V, Donadieu J, Sileo C, Barkaoui MA, Héritier S, Brisse H, et al. Chest computed tomography findings for a cohort of children with pulmonary Langerhans cell histiocytosis. Pediatr Blood Cancer 2020;67:e28496.
4. Hashimoto K, Nishimura S, Sakata N, Inoue M, Sawada A, Akagi M. Treatment Outcomes of Langerhans Cell Histiocytosis: A Retrospective Study. Medicina (Kaunas) 2021;57:356.
5. Zhang X, Zhou J, Chai X, Chen G, Guo B, Ni L, Wu P. The application of x-ray, computed tomography, and magnetic resonance imaging on 22 pediatric Langerhans cell histiocytosis patients with long bone involvement: A retrospective analysis. Medicine (Baltimore) 2018;97:e0411.
6. Chen H, Fan Q, Su M. Solitary Hard Palate Langerhans Cell Histiocytosis Demonstrated on PET/CT Scan in an Adult. Clin Nucl Med 2020;45:811-2.
7. Albano D, Bosio G, Giubbini R, Bertagna F. Role of ^{18}F-FDG PET/CT in patients affected by Langerhans cell histiocytosis. Jpn J Radiol 2017;35:574-83.
8. Kamal AF, Luthfi APWY. Diagnosis and treatment of Langerhans Cell Histiocytosis with bone lesion in pediatric patient: A case report. Ann Med Surg (Lond) 2019;45:102-9.
9. Capodiferro S, Tempesta A, Limongelli L, Ingravallo G, Maiorano E, Sfasciotti GL, Bossù M, Polimeni A, Favia G. Primary Oro-Facial Manifestations of Langerhans Cell Histiocytosis in Pediatric Age: A Bi-Institutional Retrospective Study on 45 Cases. Children (Basel) 2020;7:104.
10. Tazi A, Lorillon G, Haroche J, Neel A, Dominique S, Aouba A, Bouaziz JD, de Margerie-Melon C, Bugnet E, Cottin V, Comont T, Lavigne C, Kahn JE, Donadieu J, Chevret S. Vinblastine chemotherapy in adult patients with langerhans cell histiocytosis: a multicenter retrospective study. Orphanet J Rare Dis 2017;12:95.
11. Wang J, Song T, Wang J, Ma L, Jiang Y, Kong D,

Zhang B, Lu J. Aggressive Langerhans cell histiocytosis transformation of T cell acute lymphoblastic leukemia detected on 18F-FDG PET/CT. Eur J Nucl Med Mol Imaging 2021;48:642-3.
12. Zhao Y, Zhou Y, Tian R, Su M. Solitary Bone Langerhans Cell Histiocytosis Demonstrated on Multimodality Imaging in an Adult. Clin Nucl Med 2020;45:78-80.
13. Agarwal KK, Seth R, Behra A, Jana M, Kumar R. ^{18}F-Fluorodeoxyglucose PET/CT in Langerhans cell histiocytosis: spectrum of manifestations. Jpn J Radiol 2016;34:267-76.
14. Lee HJ, Ahn BC, Lee SW, Lee J. The usefulness of F-18 fluorodeoxyglucose positron emission tomography/computed tomography in patients with Langerhans cell histiocytosis. Ann Nucl Med 2012;26:730-7.
15. Kobayashi M, Ando S, Kawamata T, Makiyama J, Yokoyama K, Imai Y, Tojo A. Clinical features and outcomes of adult Langerhans cell histiocytosis: a single-center experience. Int J Hematol 2020;112:185-92.
16. Wu M, Niu N, Huo L. Clinical Utility of 18F-FDG PET/CT in Adult Langerhans Cell Histiocytosis: An analysis of 57 Patients. J Nucl Med 2020;61:169.
17. Szturz P, Řehák Z, Koukalová R, Adam Z, Krejčí M, Pour L, Zahradová L, Vaníček J, Nebeský T, Hájek R, Mayer J. Measuring diffuse metabolic activity on FDG-PET/CT: new method for evaluating Langerhans cell histiocytosis activity in pulmonary parenchyma. Nucl Med Biol 2012;39:429-36.
18. Hu X, Dong A, Lv S, Wang Q, Zhan X, Song X, Wang J. F-18 FDG PET/CT imaging of solitary liver Langerhans cell histiocytosis: preliminary findings. Ann Nucl Med 2012;26:436-9.
19. Narayanasamy Rajavelu T, Abimannane A, Chinnaiah Govindhareddy DK, Kayal S, Kar R. Langerhans' Cell Histiocytosis Masquerading as Caroli's Disease. J Pediatr Hematol Oncol 2020;42:e620-2.
20. Shi Y, Qiao Z, Xia C, Gong Y, Yang H, Li G, Pa M. Hepatic involvement of Langerhans cell histiocytosis in children--imaging findings of computed tomography, magnetic resonance imaging and magnetic resonance cholangiopancreatography. Pediatr Radiol 2014;44:713-8.
21. Zhu H, Ma Y, Sun L, Zhang R, Lv L, Wang A. Langerhans Cell Histiocytosis with Lymph Node Involvement Presenting as Erythroderma. Acta Derm Venereol 2019;99:99-100.
22. Reisi N, Raeissi P, Harati Khalilabad T, Moafi A. Unusual sites of bone involvement in Langerhans cell histiocytosis: a systematic review of the literature. Orphanet J Rare Dis 2021;16:1.
23. Hashimoto K, Nishimura S, Sakata N, Inoue M, Sawada A, Akagi M. Characterization of PD-1/PD-L1 immune checkpoint expression in the pathogenesis of musculoskeletal Langerhans cell histiocytosis: A retrospective study. Medicine (Baltimore) 2021;100:e27650.

Cite this article as: Luo ZH, Lu PX, Qi WL, Liao FX, Jin AF, Zen QY. Role of ^{18}F-FDG PET/CT in the diagnosis and management of patients with Langerhans cell histiocytosis. Quant Imaging Med Surg 2022;12(6):3351-3363. doi: 10.21037/qims-21-823

Supplementary

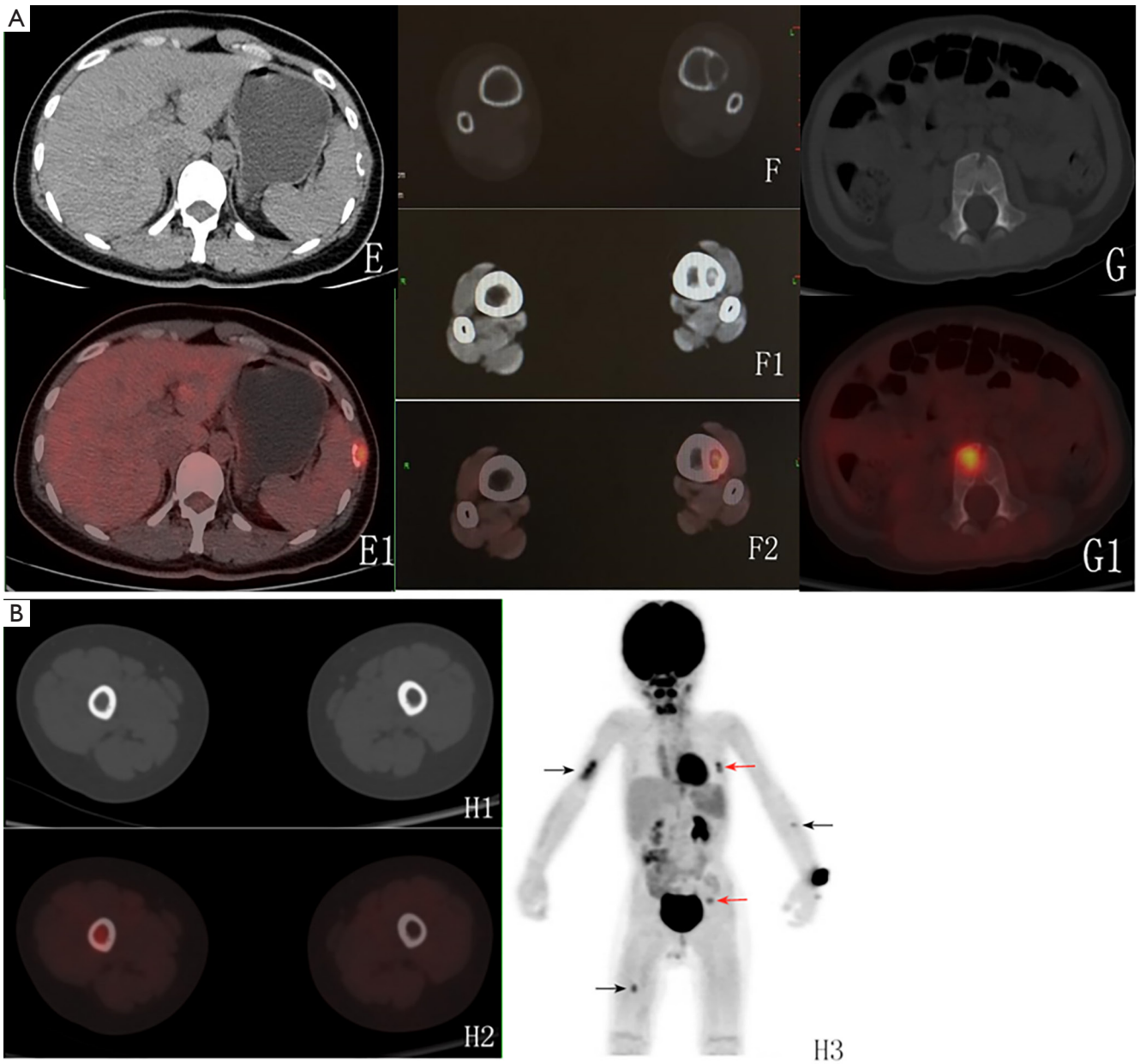

Figure S1 (A) (supplement of *Figure 3*): ^{18}F-FDG PET/CT imaging of patients (33-year-old woman) with Musculoskeletal involvement of LCH. (E,E1) Axial CT and fused image show reb lytic lesion and associated nodule with medium metabolic activity. (F,F1,F2) Axial CT (bone and soft window, fusion image) show left tibia lytic lesion with sclerosis margin and medium FDG uptake. (G,G1) Axial CT (bone window) and fused image show local hypermetabolism but no visible destruction in lumbar vertebra. (B) Images comparison of CT and PET/CT of a patients (2-year-old boy) with Musculoskeletal involvement of LCH. Axial CT (H1) showed no pathological lesions in either distal humerus. PET/CT fused image (H2) and PET MIP (H3) revealed focal FDG uptake in corresponding site, in addition, PET MIP showed multiple similar bone lesions (black arrows. Red arrows: osteolytic lesions in rib and iliac).

https://dx.doi.org/10.21037/qims-21-823

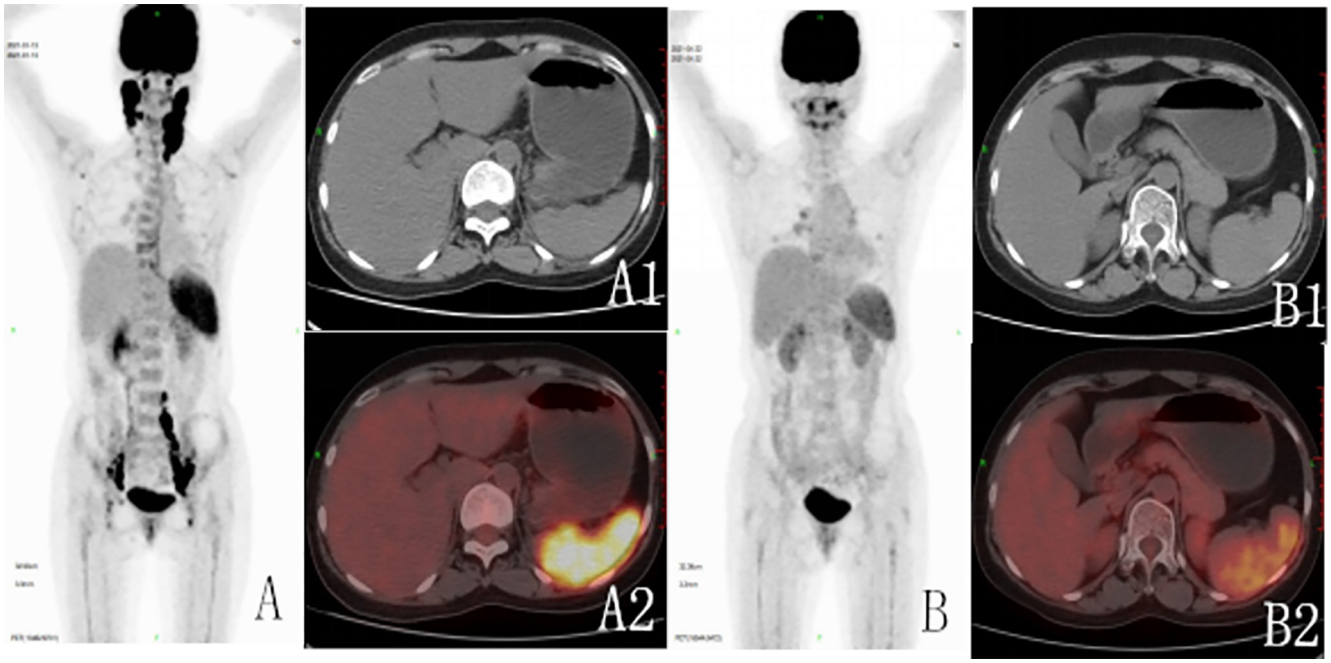

Figure S2 ^{18}F-FDG PET/CT imaging of a 35-year-old patient with lymphatic system involvement of LCH before and after treatment. (A-A2) Before treatment multiple swelling lymphadenopathy and spleen show hypermetabolism; (B-B2) cervical and basin swelling lymph nodes disappear, the metabolic activity of spleen decrease. (A,B: PET MIPs; A1,B1: Axial CTs; A2,B2: PET/CT fusion images).

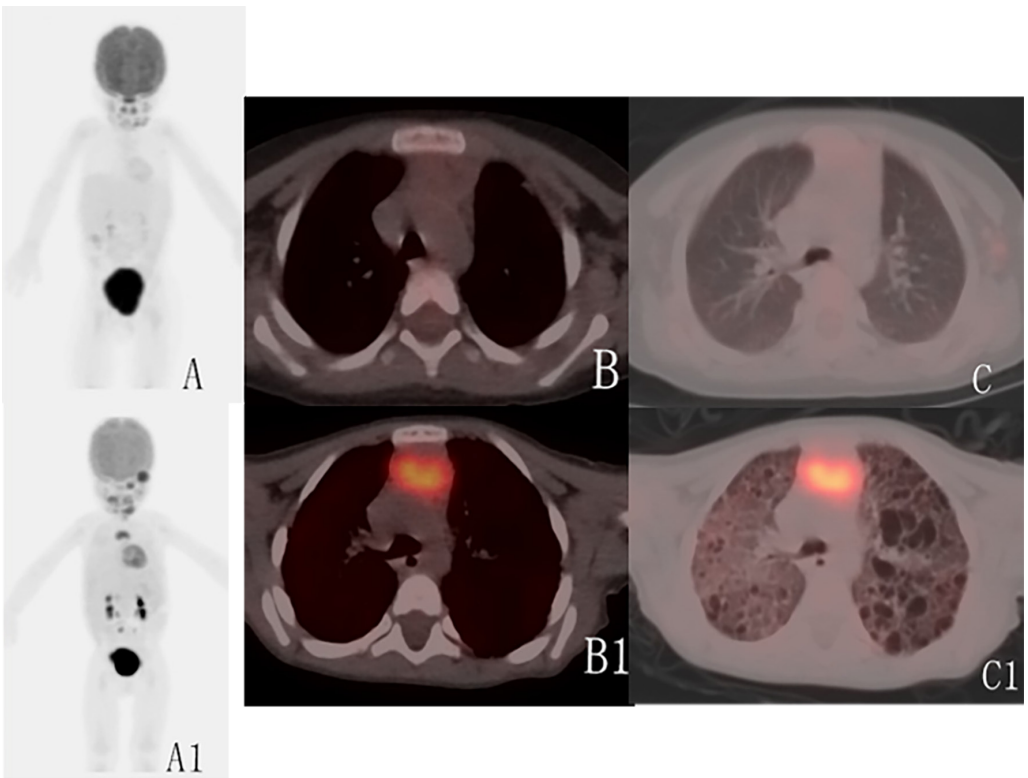

Figure S3 Comparison of PET/CT imaging of a 1-year-old girl with multi-system LCH. Imaging after chemotherapy (A-C) show metabolic activity of LCH lesions and cystic spaces in lung significantly decrease than imaging before chemotherapy (A1-C1).

https://dx.doi.org/10.21037/qims-21-823